

The Determination of α_S at Hadron Colliders

W. T. Giele

*Fermi National Accelerator Laboratory, P. O. Box 500,
Batavia, IL 60510, U.S.A.*

E. W. N. Glover

*Physics Department, University of Durham,
Durham DH1 3LE, England*

and

J. Yu

*Department of Physics and Astronomy, University of Rochester
Rochester, NY 14627, U.S.A.*

June 26, 1995

Abstract

Hadron colliders offer a unique opportunity to test perturbative QCD because, rather than producing events at a specific beam energy, the dynamics of the hard scattering is probed simultaneously at a wide range of momentum transfers. This makes the determination of α_S and the parton density functions (PDF) at hadron colliders particularly interesting. In this paper we restrict ourselves to extracting α_S for a given PDF at a scale which is directly related to the transverse energy produced in the collision. As an example, we focus on the single jet inclusive transverse energy distribution and use the published '88-'89 CDF data with an integrated luminosity of 4.2 pb^{-1} . The evolution of the coupling constant over a wide range of scales (from 30 GeV to 500 GeV) is clearly shown and is in agreement with the QCD expectation. The data to be obtained in the current Tevatron run (expected to be well in excess 100 pb^{-1} for both the CDF and $D\bar{O}$ experiments) will significantly decrease the experimental errors.

1 Introduction

Hadronic collisions at the Fermilab TEVATRON offer excellent opportunities to study QCD over a broad range of momentum transfers ranging from a few GeV in the transverse momentum distribution of the Z boson up to almost half of the beam energy in the single jet inclusive transverse energy distribution. While the experiments at LEP and HERA have set well defined goals for QCD studies, hadron colliders tend to be thought of as discovery machines probing the high energy frontier. For example, at Fermilab, the major effort has been concentrated on the study of the Top Quark and W -mass measurements. In this paper, we try to redress this imbalance and outline a possible goal for QCD studies at hadron colliders. Achieving this goal will give both a rigorous test of QCD and a reduction of the experimental systematic errors in the other studies at Fermilab.

One possible goal of QCD studies at the Main Injector [1] is to use the QCD data set to determine the input parameters of the theory, in other words, α_S and the parton density functions (PDF's), *without* input from other experiments.¹ This should also allow the determination of the gauge symmetry responsible for the strong interactions thereby extending similar measurements at LEP [2]. In order to achieve this goal, we need to make several intermediate steps to identify problems in both experiments and theory. The run 1A and 1B data can be used to gain experience in how to analyze the data and to identify those distributions which can be measured accurately and calculated reliably. We will break the program into four steps with each phase contributing to a better understanding of QCD at hadron colliders.

In the first phase we use the PDF's obtained from global analyses [3, 4, 5, 6] and the associated $\alpha_S(M_Z)$ as input parameters. Then by comparing data to theory we can identify those cross sections which are most sensitive to the input parameters. Using run 1A data it has become clear that certain distributions will be better than others in determining the parton density functions and α_S . For example, the parton density functions can be constrained from di-jet data using angular correlations [7], the same-side to opposite-side ratio [8, 9, 10] and via the triply differential cross section [11, 12, 13, 14, 15] while the strong coupling can be determined from vector boson production at large transverse momentum [16, 17, 18].

In the second phase we will assume a given PDF set as being correct and extract α_S . Measuring α_S at a hadron collider is rather different than measuring α_S at LEP with the most important difference being the fact that one can measure α_S from momentum transfers as low as a few GeV all the way up to 500 GeV simultaneously and with high statistics [15]. In this paper we will use the one-jet inclusive transverse energy distribution measured from the '88-'89 CDF data with an integrated luminosity of 4.2 pb^{-1} to illustrate this method.

¹Note that the range of x and Q^2 probed in hadron-hadron collisions is rather different from that probed at HERA.

The analysis can be repeated for the current CDF and DØ data sets increasing the integrated luminosity to well over 100 pb^{-1} . These increased statistics will have a major impact on both the statistical and systematic error relative to the '88-'89 data set. The results in this paper are therefore just an illustration of the method and no detailed effort has been made to determine the experimental systematic errors thoroughly. This would require detailed knowledge of the correlation matrix for the systematic error which is not readily available. While the value of α_S extracted in this way cannot be considered on the same footing as that measured at LEP because the PDF's themselves are dependent on α_S , this measurement will nevertheless provide valuable information. For example, the extracted α_S must be consistent with the α_S used in the PDF, or else the data is incompatible with this particular set. If one finds that the extracted α_S is compatible with the PDF the measurement gives an additional constraint on the PDF at large x and Q^2 . Further, one can also study the evolution of α_S for a wide range of momentum transfers.²

In the third phase we determine both the PDF's and α_S simultaneously using the triply differential di-jet inclusive distributions [8, 11, 12], possibly including flavor tagging, yielding an α_S that is completely independent of the DIS data set. In principle the measurement is very simple, the parton fractions are determined by summing over the rapidity weighted transverse momenta of the particles produced by the hard scattering, $x_{1,2} = (\sum_i E_T^i e^{\pm\eta_i})/\sqrt{S}$ [13, 14]. However, since it is impossible to measure and identify all the particles associated with the hard scattering, we are forced to rely on higher order calculations to estimate the unobserved radiation. It might therefore be prudent to separate this phase into two steps by first determining the distribution of gluons in the proton and assuming the distribution of charged partons is determined by the DIS data set. The reason for this is that in deep inelastic scattering the virtual photon directly probes the charged parton distributions. The effects of the gluon distribution enter first at next-to-leading order and cause, for example, scaling violations in the slope of F_2 . On the other hand, in hadron colliders, the gluon density enters at lowest order and a more direct measurement should be possible. For example, by using the triply differential di-jet data one probes the gluon distribution directly with essentially unlimited statistics. After the gluon distribution has been successfully extracted in this manner, one can include the triply differential V + jet data (where $V = W, Z, \gamma$) to extract the charged PDF's. A successful determination of both α_S and the PDF's from the hadronic data set over a wide range of momentum transfers would be an important test of QCD and its consistent description using perturbative QCD. The measured PDF's and α_S can directly be used in other physics analyses at hadron colliders thereby reducing the experimental systematic uncertainties considerably.

After completing the program outlined above, one can then test QCD and the gauge

²An alternative approach has been followed by UA2 [16] and is now being pursued actively by both CDF and DØ. Here, one uses PDF's which are fitted to the Deep Inelastic Scattering (DIS) data set for several values of $\alpha_S(M_Z)$. This allows simultaneous variation of α_S in the PDF and matrix elements leading to a consistent $\alpha_S(M_Z)$ extracted from the combined DIS and hadronic data set which can then be directly compared to the LEP value of α_S .

group responsible for the strong interactions from first principles. This would be the final phase and is quite similar to the efforts at LEP [2]. Of course, in hadron colliders there is the additional interesting feature that the PDF and its evolution are also predicted by the gauge group. All together, this will give an accurate measurement of the gauge nature of the strong interactions and quantify how well the data set fits the QCD theory.

This program is an achievable goal for the Main Injector run where, because of the expected high luminosities and small experimental errors, we expect to see deviations from the next-to-leading order predictions, even without assuming new physics. This makes it crucial we understand the uncertainties related to the PDF's and QCD very well. By determining α_S and the PDF's within one experiment one can identify which parts of the theoretical calculation are important and try to improve them. Furthermore, if significant deviations from next-to-leading order show up, it will be easier to identify possible problems in the theory or conclude that the deviations are due to new physics. An added bonus is that the PDF's and α_S determined at large x and Q^2 can immediately be used in other physics analyses which naturally occur at similar x and Q^2 values, thereby further reducing the systematic errors associated with luminosity, α_S , PDF's, etc. Finally one can test QCD in a very rigorous manner by comparing the parton density functions determined in both deep inelastic scattering and the hadron collider at a common scale. Eventually, this might lead to a unified global fit of the PDF's to *all* hadronic data.

In sec. 2 we will discuss the theoretical issues involved in extracting α_S and will set up a general framework to extract α_S from a given data set. This framework is applied in sec. 3 to the one-jet inclusive transverse energy distribution. Section 4 contains a brief description of the CDF data, while the detailed results for the determination of α_S and it's evolution are presented in sec. 5. The conclusions summarize our main results and briefly discuss the prospects for measuring α_S at the TEVATRON.

2 Theoretical considerations

2.1 Running coupling constants

In order to calculate an observable \mathcal{O}^{data} within perturbative QCD we have to introduce the renormalization scale μ_R . However, no matter what scale we choose, it cannot affect the prediction for the physical observable. This statement can be formalized in the renormalization group equation for the running coupling constant $\alpha_S(\mu_R)$. Both the coupling constant and the matrix element coefficients depend on the renormalization scale while the physical quantity does not. This means that when measuring α_S we have to specify the renormalization scale so that the extracted α_S will be the value of α_S at that particular renormalization scale. Of course, all possible choices of the renormalization scale are related to each other

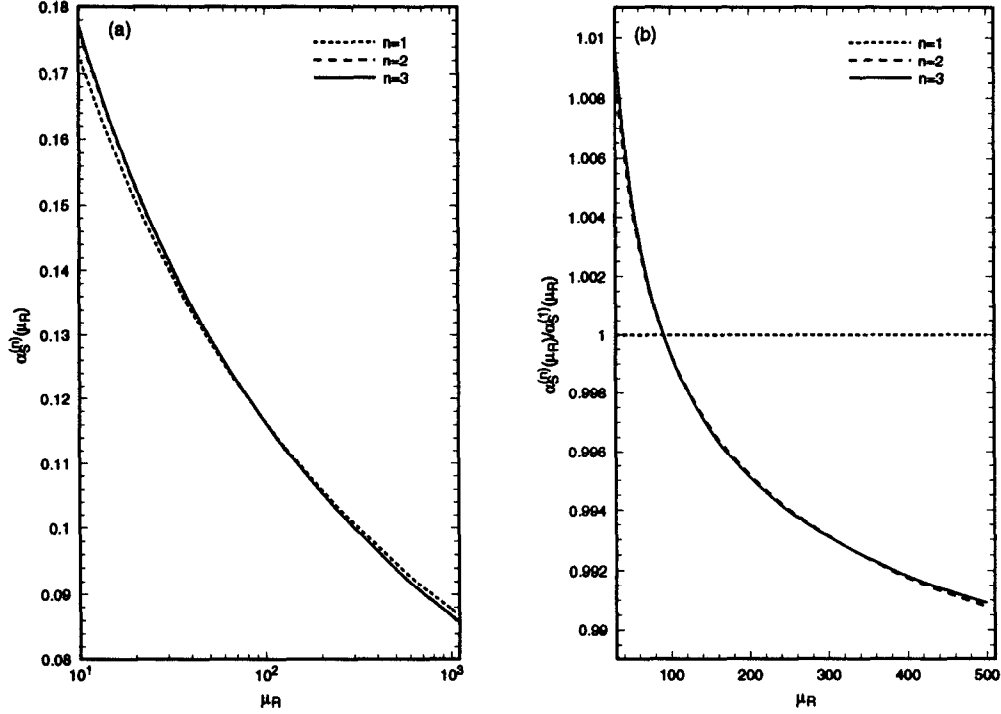


Figure 1: Comparison between the 1st, 2nd and 3rd order running of $\alpha_S(\mu_R)$ for $\alpha_S(M_Z) = 0.118$. Fig. 1a shows $\alpha_S^{(n)}(\mu_R)$ from 10 GeV to 1000 GeV while Fig. 1b gives the relative change with respect to the 1st order running over the relevant energy range from 30 GeV to 500 GeV.

by virtue of the renormalization group equation. Relative to a fixed scale, M_Z , the n -loop running coupling constant at scale $\mu_R = \lambda M_Z$ is given by,

$$\alpha_S(\mu_R) = \frac{\alpha_S(M_Z)}{1 + \alpha_S(M_Z)L^{(n)}(\lambda)} \quad (1)$$

where,

$$L^{(1)}(\lambda) = b_0 \log(\lambda), \quad (2)$$

$$L^{(2)}(\lambda) = (b_0 + b_1 \alpha_S(M_Z)) \log(\lambda), \quad (3)$$

$$L^{(3)}(\lambda) = (b_0 + b_1 \alpha_S(M_Z) + b_2^{\overline{MS}} \alpha_S^2(M_Z)) \log(\lambda) - \frac{b_0 b_1}{2} \alpha_S^2(M_Z) \log^2(\lambda). \quad (4)$$

The first three coefficients of the Callan-Symanzik β -function are given by [19, 20, 21],

$$\begin{aligned} b_0 &= \frac{11N_c - 2n_f}{6\pi}, \\ b_1 &= \frac{34N_c^2 - 13N_c n_f + 3n_f/N_c}{24\pi^2}, \\ b_2^{\overline{MS}} &= \frac{5714N_c^3 - 3391N_c^2 n_f + 224N_c n_f^2 + 507n_f + 54n_f/N_c^2 - 66n_f^2/N_c}{3456\pi^3}, \end{aligned} \quad (5)$$

where N_c is the number of colors and n_f the number of active flavors.³ Note that while b_0 and b_1 are independent of the renormalization scheme, b_2 is renormalization scheme dependent. The expression given here is for the $\overline{\text{MS}}$ scheme which we use throughout the paper.

For the processes we will consider, the momentum transfer ranges from 30 GeV up to around 500 GeV. In Fig. 1a we show the running α_S in this range for $\alpha_S(M_Z) = 0.118$. We see that the differences between the evolution at different orders is rather small in the relevant energy range, essentially because $\alpha_S(M_Z)$ and $\log(\lambda)$ are both small. To see the differences more clearly, Fig. 1b shows the relative change in $\alpha_S(\mu_R)$ with respect to the 1st order evolution. The percentage change between 1st and 2nd order evolution in the range from 30 GeV to 500 GeV is less than $\pm 1\%$ and could be safely ignored with the present level of theoretical and experimental accuracy. In addition, the difference between 2nd and 3rd order is completely negligible. Therefore, in the rest of the paper we will use the 2-loop evolution as given in eq. 3.

2.2 Extracting α_S

Measuring α_S from an observable \mathcal{O}^{data} is, in principle, rather straightforward *provided* higher twist effects and other non-perturbative effects are small so that the perturbative expansion can be considered a reliable estimate of the cross section. In other words, we calculate the perturbative expansion \mathcal{O}^{pert} and equate it with the data,

$$\mathcal{O}^{data} \equiv \mathcal{O}^{pert}. \quad (6)$$

For example, for the single jet inclusive transverse energy distribution,

$$\mathcal{O} = \frac{d\sigma}{dE_T},$$

there is a good agreement between perturbative calculations and the data over 7 orders of magnitude in the cross section in the range $30 \leq E_T \leq 500$ GeV [22, 23]. By comparing data with theory for each E_T -bin, we make many independent measurements of α_S at a specified renormalization scale assuming no correlated bin-to-bin experimental systematic errors.

The perturbative expansion can be written,

$$\mathcal{O}^{pert} = \alpha_S^m(\mu_R) \hat{\mathcal{O}}^{(0)} K^{(\infty)}(\alpha_S(\mu_R), \mu_R/Q_R), \quad (7)$$

where the scale Q_R is the characteristic scale for the observable under consideration which will be the transverse energy of the jet for the single jet inclusive transverse energy distribution. The Born-prediction is given by $\alpha_S^m(\mu_R) \hat{\mathcal{O}}^{(0)}$ and all the higher order corrections are

³The numerical values for the β -function coefficients are: $b_0 = 1.2202$, $b_1 = 0.4897$ and $b_2^{\overline{\text{MS}}} = 0.1913$ for $N_c = 3$ and $n_f = 5$.

contained in the K -factor,

$$K^{(n)}(\alpha_S(\mu_R), \mu_R/Q_R) = 1 + \sum_{l=1}^n \alpha_S^l(\mu_R) k_l(\mu_R/Q_R). \quad (8)$$

For the single jet inclusive transverse energy distribution, $m = 2$ and the K -factor is currently known up to next-to-leading order, giving $K^{(1)}$.

Once the K -factor has been calculated up to the n -th order in α_S , the first step in extracting the n -th order $\alpha_S^{(n)}$ is to determine the leading order $\alpha_S^{(0)}$ together with its experimental uncertainties. This is simply given by the ratio of the data over the leading order coefficient $\hat{O}^{(0)}$

$$\alpha_S^{(0)} = \sqrt[m]{\frac{\mathcal{O}^{data}}{\hat{O}^{(0)}}}, \quad (9)$$

and does not depend on the renormalization scale.⁴

While the determination of the leading order α_S has no useful theoretical interpretation it is nevertheless a very convenient manner in which to parametrize the data. In principle, all we need from an experiment is the leading order α_S as given in eq. 9 together with the experimental errors. From here we can determine $\alpha_S^{(n)}$ values without referring back to the original data. For example, given $K^{(n)}$, the n -th order α_S is given by,

$$\alpha_S^{(n)}(\mu_R) = \frac{\alpha_S^{(0)}}{\sqrt[m]{K^{(n)}(\alpha_S^{(n)}(\mu_R), \mu_R/Q_R)}}, \quad (10)$$

so that $\alpha_S^{(n)}(\mu_R)$ are just the roots of the $(m + n)$ -th order polynomial,

$$[\alpha_S^{(n)}(\mu_R)]^m \left(1 + \sum_{l=1}^n [\alpha_S^{(n)}(\mu_R)]^l k_l(\mu_R/Q_R) \right) - [\alpha_S^{(0)}]^m = 0. \quad (11)$$

2.3 Theoretical Uncertainty

For the processes of interest, only the first order corrections are currently known. Therefore, we use the leading order $\alpha_S^{(0)}$ (with experimental errors) and solve the $(m + 1)$ th order polynomial,

$$k_1(\mu_R/Q_R)[\alpha_S^{(1)}(\mu_R)]^{(m+1)} + [\alpha_S^{(1)}(\mu_R)]^m - [\alpha_S^{(0)}]^m = 0, \quad (12)$$

with $\mu_R = \mu_0$ to find $\alpha_S^{(1)}(\mu_0)$. For the single jet inclusive transverse energy distribution, we choose $\mu_0 = Q_R = E_T$.

⁴For hadronic collisions the Born term $\hat{O}^{(0)}$ will have an implicit dependence on the factorization scale, μ_F . Throughout, we specify $\mu_F = Q_R$.

To estimate the theoretical uncertainty we can extract α_S at renormalization scale $\mu_R = \lambda\mu_0$ which we subsequently evolve back to scale μ_0 using the 2-loop renormalization group running of α_S . Quantitatively this means we solve eq. 12 with $\mu_R = \lambda\mu_0$ and determine,

$$\alpha_S(\mu_0; \mu_R = \lambda\mu_0) = \frac{\alpha_S(\lambda\mu_0)}{1 + \alpha_S(\lambda\mu_0)L^{(2)}(1/\lambda)}. \quad (13)$$

By defining,

$$\frac{\Delta\alpha_S(\lambda)}{\alpha_S} \equiv \frac{\alpha_S(\mu_0; \mu_R = \lambda\mu_0) - \alpha_S(\mu_0; \mu_R = \mu_0)}{\alpha_S(\mu_0; \mu_R = \mu_0)}, \quad (14)$$

we can estimate the theoretical uncertainty in α_S .

The reason $\Delta\alpha_S$ is non-zero is due to the fact that the NLO coefficient $k_1(\mu_R = \lambda\mu_0)$ is only the first order correction and rest of the higher order corrections are neglected. The behavior of k_1 under renormalization scale changes is,

$$k_1(\mu_R = \lambda\mu_0) = k_1(\mu_R = \mu_0) + mb_0 \log(\lambda). \quad (15)$$

This shift changes the solution of eq. 12 giving us $\alpha_S(\lambda\mu_0)$. However, evolving back to $\mu_R = \mu_0$ using eq. 13 does not exactly match the change due to eq. 15. In fact the shift in α_S due to this mismatch has a relatively simple form for small $\log(\lambda)$,

$$\frac{\Delta\alpha_S(\lambda)}{\alpha_S} \sim \alpha_S^2 \left(\frac{(m+1)b_0k_1(\mu_R = \mu_0)}{m + (m+1)\alpha_Sk_1(\mu_R = \mu_0)} + b_1 \right) \log(\lambda) + \mathcal{O}(\log^2(\lambda)). \quad (16)$$

To extract the central value of $\alpha_S(\mu_0)$ and its theoretical uncertainty we can follow many different procedures. We will outline two of them here.

Method I

The first procedure is rather straightforward. We take $\mu_R = \mu_0$ as the central scale and vary the renormalization scale between $\mu_R = \mu_0/2$ and $\mu_R = 2\mu_0$ to estimate the uncertainty. Explicitly this means,

$$\begin{aligned} \alpha_S^{(1)}(\mu_0) &= \frac{1}{2} \left(\alpha_S(\mu_0; \mu_R = 2\mu_0) + \alpha_S(\mu_0; \mu_R = \mu_0/2) \right), \\ \Delta\alpha_S^{(1)}(\mu_0) &= \frac{1}{2} \left(\alpha_S(\mu_0; \mu_R = 2\mu_0) - \alpha_S(\mu_0; \mu_R = \mu_0/2) \right). \end{aligned} \quad (17)$$

Method II

The second procedure is based on the fact that $\Delta\alpha_S/\alpha_S$ has a minimum. This occurs when $\lambda = \lambda_0 = \exp(-k_1(\mu_R = \mu_0)/mb_0)$ so that the first order correction vanishes,

$k_1(\mu_R = \lambda_0\mu_0) = 0$ and $\alpha_S^{(0)} = \alpha_S^{(1)}(\mu_R = \lambda_0\mu_0)$. Now we can define $\alpha_S^{(1)}(\mu_0)$ and the theoretical uncertainty in the following manner,

$$\begin{aligned}\alpha_S^{(1)}(\mu_0) &= \frac{1}{2}\left(\alpha_S(\mu_0; \mu_R = \mu_0) + \alpha_S(\mu_0; \mu_R = \lambda_0\mu_0)\right), \\ \Delta\alpha_S^{(1)}(\mu_0) &= \frac{1}{2}\left(\alpha_S(\mu_0; \mu_R = \mu_0) - \alpha_S(\mu_0; \mu_R = \lambda_0\mu_0)\right).\end{aligned}\quad (18)$$

There are two major differences between the two methods of estimating the theoretical uncertainty. First, the estimated theoretical uncertainty is generally larger in method I than in method II and second, the central value of $\alpha_S(\mu_0)$ using method II is slightly lower, but by construction it lies within the range of uncertainty of method I.

3 The one-jet inclusive transverse energy distribution

The one-jet inclusive transverse energy distribution ($d\sigma/dE_T$) has a straightforward interpretation: the transverse energy of the leading jet (E_T) is directly related to the impact parameter b_{impact} (or the distance scale) in the underlying hard parton-parton scattering by the relation

$$\left(\frac{b_{impact}}{1 \text{ fm}}\right) = 0.0507 \times \left(\frac{E_T}{100 \text{ GeV}}\right)^{-1}. \quad (19)$$

Therefore by studying this particular distribution we probe rather directly the physics over a wide range of distance scales within one single measurement. For the published CDF data, the transverse energies range from 30 GeV up to 500 GeV. In other words, we probe the dynamics of the parton-parton scattering from a distance scale of 0.169 fm all the way down to 0.01 fm. The obvious quantity to study is therefore α_S extracted at renormalization scale $\mu_R = E_T$. Subsequently we can test QCD by comparing the measured α_S at the different distance scales with the running α_S predicted by QCD. The comparison will be sensitive to new physics, the most obvious being substructure of the quarks. However, deviations from QCD at small distance scales will also show up as violations of the running of α_S . To perform the comparison with QCD we will use two methods, each of which has its own interest. The first one assumes the evolution is correctly given by QCD to extract α_S at a common scale, $\mu_R = M_Z$, while the second method quantifies deviations from purely QCD-like evolution.

3.1 The QCD-fit

In the first method we *assume* the correctness of QCD to describe the parton-parton scattering at all distance scales relevant in this measurement. This enables us to extract the

best possible value of $\alpha_S(M_Z)$ using a given data set. Each E_T -bin in the differential cross section gives an independent measurement of $\alpha_S(E_T)$ which we subsequently can evolve to $\alpha_S(M_Z)$ using the renormalization group equation. The published CDF data set has 38 individual E_T -bins, and therefore yields 38 independent measurements of $\alpha_S(M_Z)$, so that the statistical error will be negligible compared to the common systematic error which has two components. The first is the calorimeter response correction together with fragmentation/hadronization effects and the second is the luminosity uncertainty. The luminosity uncertainty can be reduced using the W -boson production cross section (σ_W) as a luminosity measurement. Experimentally this simply involves counting the number of W -boson events and normalizing $d\sigma/dE_T$ respectively, i.e. we study $1/\sigma_W d\sigma/dE_T$ so that the luminosity uncertainty cancels. Theoretically, σ_W is the best known cross section at hadron colliders, known up to 2-loop QCD corrections [24]. Therefore $1/\sigma_W d\sigma/dE_T$ can be calculated consistently order by order in perturbative QCD and compared to experiment to extract α_S . This method of normalizing the cross section can easily be generalized to all observables.

3.2 The Best-fit

It may turn out that the measured $\alpha_S(M_Z)$ is not independent of the E_T values it was extracted from. This indicates either deficiencies in the input PDF or, more interestingly, deviations from the underlying QCD theory. Parametrizing possible deviations from the QCD condition $\partial\alpha_S(M_Z; \mu_R = E_T)/\partial E_T = 0$ will give us an excellent check on the theory. We therefore quantify deviations from QCD by allowing $\partial\alpha_S(M_Z; \mu_R = E_T)/\partial E_T = f(E_T) \neq 0$. The size of the deviation $f(E_T)$ and its uncertainty will tell us how well the data set fits QCD. More interestingly, by evolving the fit to $\alpha_S(M_Z; \mu_R = E_T)$ back to $\alpha_S(E_T)$ we obtain the “Best-fit” prediction for the evolution of α_S . By extrapolating the fit to larger and smaller scales we find the permissible range of evolution for $\alpha_S(\mu_R)$ allowing for small deviations from QCD in the current data set. We can then compare with α_S measurements at different energy scales and see how compatible the deviations are with the other measurements, in particular the slower running that may be suggested by the low energy data [25]. While the systematic error dominates in the “QCD-fit” method, here the systematic error (including the theoretical uncertainty) will merely affect the overall normalization of the α_S evolution and not the shape. In fact by normalizing the curve to the world average value of $\alpha_S(M_Z)$ we can completely remove the systematic error.

4 The CDF data

The CDF data used in this analysis is from the '88-'89 TEVATRON collider run at Fermilab which yielded an integrated luminosity of 4.2 pb^{-1} . The data was taken from the preprint version [26] of the published letter [23]. The preprint tabulates the results together with the

separated statistical and systematic errors. Unfortunately the error-analysis in the current paper is limited by the fact that the published results do not have the necessary detailed discussion of the systematic errors needed for a more rigorous error treatment. We will use an ad-hoc procedure to separate a common systematic error and a bin-by-bin statistical error. Also the removal of the luminosity error using the W -boson cross section cannot be applied, as this would require a careful simultaneous study of the W -boson and jet data. However, both the CDF and DØ collaborations can incorporate a proper error analysis and removal of the luminosity error using the new run 1A/B data sets. Our purpose here is to illustrate the methods rather than produce a definitive measurement and error analysis.

The one-jet inclusive transverse energy distribution of CDF is constructed by including *all* the jets, which are defined according to the Snowmass algorithm with a conesize of 0.7 [27], in the pseudo-rapidity range between 0.1 and 0.7. This means that this particular distribution is not exactly the transverse energy distribution of the leading jet as would be preferred for the α_S measurement, but contains some softer jets. However, although small deviations from the leading jet E_T distribution can be expected at small E_T , for high- E_T bins there is virtually no difference between the two distributions.

Some of the features of the particular data taking for the '88-'89 run will be reflected in the α_S measurement. First of all, the statistical error is affected by the different event triggers, each with its own prescaling factor. The off-line E_T cuts (ensuring 98% efficiency in the data taking) for the three triggers are 35 GeV (with prescaling factor 1 per 300 events), 60 GeV (1 per 30 events) and 100 GeV (not prescaled) [23]. This means the statistical errors fall into three distinct regions which eventually will be reflected in the statistical error on α_S . Second, the systematic error is due to the luminosity measurement and the detector response combined with the hadron distribution within the jets (which is modelled by fragmentation/hadronization Monte Carlo's). The systematic error quoted contains all these uncertainties and most of the error will be common to all the bins. Apart from the luminosity error, the systematic error falls into two separate regions. Below $E_T = 80$ GeV, the systematic error is large, decreasing from as high as $\pm 60\%$ at 35 GeV to $\pm 22\%$ at 80 GeV. As a result, the α_S measurement below 80 GeV is strongly affected by short range correlated systematic errors. For $E_T > 80$ GeV, however, the systematic error is fairly constant with a typical value of $\pm 22\%$, making the short range systematic error correlations small. Again these characteristics of the data will eventually be reflected in the measured α_S .

5 Determining α_S

To extract α_S we use the next-to-leading order parton level Monte Carlo JETRAD [28] which is based on the techniques described in refs. [29, 30] and the matrix elements of ref. [31]. The cuts and jet algorithm applied directly to the partons, were modelled as closely as possible

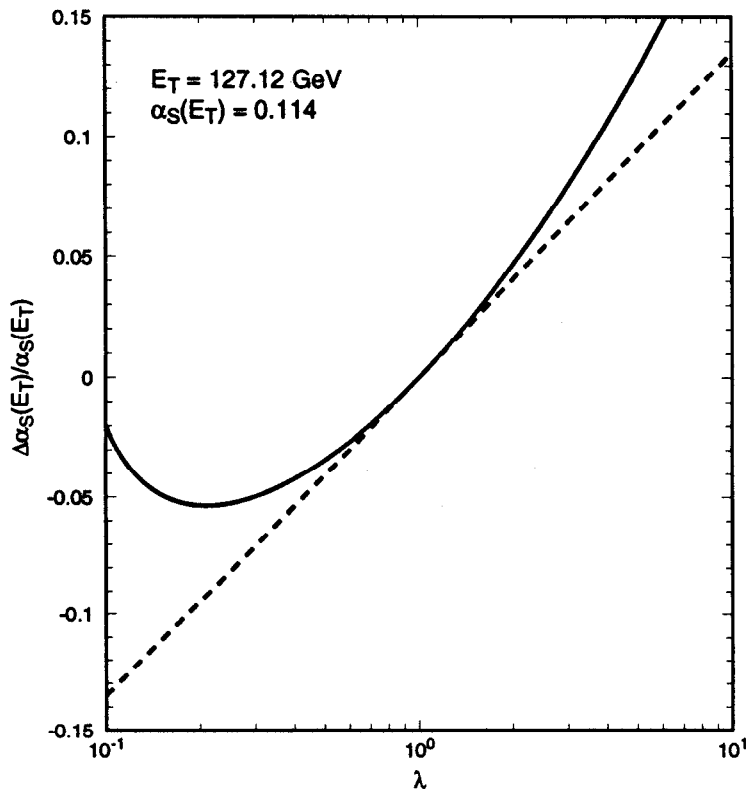


Figure 2: The uncertainty in $\alpha_S(E_T)$ due to variation in the renormalization scale (solid line). Also shown is the logarithmic tangent of eq. 16 (dashed line) which has a simple analytic form.

to the experimental set-up. Using the Monte Carlo we calculated the Born coefficient $\hat{O}^{(0)}$ and the next-to-leading order coefficient $k^{(1)}$ as defined in eqs. 7 and 8 for the MRSA' PDF set of ref. [6]. These distribution functions use the low- x F_2 data from the 1993 data taking run at HERA. However, we are mainly concerned with x values typically greater than few $\times 10^{-2}$, and there is little impact from HERA data in this range. To see this, we also consider the older MRSD0' and MRSD-' parameterisations [3]. Using eq. 9 we determine the leading order $\alpha_S^{(0)}$ from the CDF data including the statistical and systematic errors. The results are listed in Table 1 together with the next-to-leading order coefficients determined at a renormalization/factorization scale equal to the E_T value of the bin and the Monte Carlo integration error. This table contains all the information needed to extract the next-to-leading order α_S .

5.1 Measurement of $\alpha_S^{(1)}(E_T)$

Finally we are in a position to determine the next-to-leading order $\alpha_S^{(1)}$ and the associated theoretical uncertainty. We combine the experimental statistical and systematic errors on the leading order $\alpha_S^{(0)}$ in quadrature and solve eq. 12 with $m = 2$ and $\mu_0 = E_T$ to extract $\alpha_S^{(1)}(E_T)$.

E_T (GeV)	MRSA'			
	$\alpha_S^{(0)}$	k_1	$\alpha_S^{(1)}(E_T)$	$\alpha_S^{(1)}(M_Z) \pm 0.008$
35.48	$0.163 \pm 0.003^{+0.027}_{-0.049}$	2.90 ± 0.24	$0.138 \pm 0.028 \pm 0.007$	$0.118 \pm 0.013 \pm 0.005$
41.63	$0.154 \pm 0.001^{+0.025}_{-0.044}$	2.94 ± 0.26	$0.131 \pm 0.026 \pm 0.006$	$0.116 \pm 0.013 \pm 0.005$
47.61	$0.149 \pm 0.001^{+0.024}_{-0.039}$	3.18 ± 0.29	$0.126 \pm 0.023 \pm 0.006$	$0.114 \pm 0.011 \pm 0.005$
53.54	$0.149 \pm 0.002^{+0.022}_{-0.033}$	3.42 ± 0.27	$0.125 \pm 0.020 \pm 0.006$	$0.115 \pm 0.009 \pm 0.005$
59.93	$0.143 \pm 0.003^{+0.021}_{-0.029}$	3.04 ± 0.24	$0.122 \pm 0.019 \pm 0.005$	$0.115 \pm 0.009 \pm 0.004$
66.23	$0.144 \pm 0.003^{+0.019}_{-0.024}$	3.34 ± 0.23	$0.122 \pm 0.016 \pm 0.005$	$0.116 \pm 0.007 \pm 0.005$
72.29	$0.145 \pm 0.001^{+0.019}_{-0.021}$	2.80 ± 0.25	$0.125 \pm 0.015 \pm 0.005$	$0.121 \pm 0.006 \pm 0.005$
78.15	$0.147 \pm 0.002^{+0.018}_{-0.018}$	3.11 ± 0.24	$0.125 \pm 0.013 \pm 0.005$	$0.122 \pm 0.005 \pm 0.005$
83.81	$0.153 \pm 0.002^{+0.018}_{-0.016}$	3.57 ± 0.21	$0.127 \pm 0.012 \pm 0.006$	$0.125 \pm 0.004 \pm 0.006$
89.31	$0.148 \pm 0.002^{+0.018}_{-0.016}$	3.35 ± 0.25	$0.125 \pm 0.013 \pm 0.006$	$0.124 \pm 0.005 \pm 0.006$
94.82	$0.147 \pm 0.003^{+0.018}_{-0.016}$	3.39 ± 0.22	$0.123 \pm 0.013 \pm 0.006$	$0.124 \pm 0.005 \pm 0.006$
100.19	$0.145 \pm 0.003^{+0.018}_{-0.016}$	3.73 ± 0.23	$0.120 \pm 0.012 \pm 0.005$	$0.122 \pm 0.005 \pm 0.006$
105.60	$0.144 \pm 0.004^{+0.017}_{-0.016}$	3.45 ± 0.23	$0.121 \pm 0.012 \pm 0.005$	$0.124 \pm 0.005 \pm 0.006$
111.04	$0.143 \pm 0.004^{+0.017}_{-0.015}$	3.28 ± 0.23	$0.121 \pm 0.012 \pm 0.005$	$0.125 \pm 0.005 \pm 0.006$
116.44	$0.135 \pm 0.001^{+0.017}_{-0.016}$	3.77 ± 0.22	$0.113 \pm 0.012 \pm 0.005$	$0.118 \pm 0.005 \pm 0.005$
121.76	$0.136 \pm 0.001^{+0.017}_{-0.016}$	3.52 ± 0.22	$0.115 \pm 0.012 \pm 0.005$	$0.120 \pm 0.005 \pm 0.005$
127.12	$0.135 \pm 0.001^{+0.017}_{-0.016}$	3.50 ± 0.21	$0.114 \pm 0.012 \pm 0.005$	$0.120 \pm 0.006 \pm 0.005$
132.49	$0.134 \pm 0.001^{+0.017}_{-0.016}$	3.77 ± 0.23	$0.113 \pm 0.012 \pm 0.005$	$0.119 \pm 0.005 \pm 0.005$
137.77	$0.135 \pm 0.002^{+0.017}_{-0.016}$	3.44 ± 0.20	$0.114 \pm 0.012 \pm 0.005$	$0.121 \pm 0.006 \pm 0.005$
143.05	$0.134 \pm 0.002^{+0.017}_{-0.016}$	3.77 ± 0.22	$0.112 \pm 0.012 \pm 0.005$	$0.120 \pm 0.006 \pm 0.005$
148.48	$0.134 \pm 0.002^{+0.016}_{-0.015}$	4.10 ± 0.22	$0.111 \pm 0.011 \pm 0.005$	$0.119 \pm 0.005 \pm 0.005$
153.71	$0.132 \pm 0.002^{+0.016}_{-0.015}$	3.78 ± 0.22	$0.111 \pm 0.012 \pm 0.004$	$0.120 \pm 0.006 \pm 0.005$
158.93	$0.133 \pm 0.003^{+0.016}_{-0.015}$	3.54 ± 0.20	$0.112 \pm 0.011 \pm 0.004$	$0.122 \pm 0.006 \pm 0.005$
164.25	$0.133 \pm 0.003^{+0.016}_{-0.015}$	4.26 ± 0.19	$0.110 \pm 0.011 \pm 0.005$	$0.119 \pm 0.005 \pm 0.006$
171.89	$0.135 \pm 0.003^{+0.016}_{-0.015}$	3.95 ± 0.16	$0.113 \pm 0.011 \pm 0.005$	$0.124 \pm 0.005 \pm 0.006$
182.20	$0.135 \pm 0.003^{+0.015}_{-0.014}$	3.98 ± 0.14	$0.112 \pm 0.011 \pm 0.005$	$0.125 \pm 0.005 \pm 0.006$
193.04	$0.128 \pm 0.004^{+0.016}_{-0.015}$	4.05 ± 0.14	$0.107 \pm 0.011 \pm 0.004$	$0.119 \pm 0.006 \pm 0.005$
203.47	$0.116 \pm 0.005^{+0.017}_{-0.016}$	3.75 ± 0.14	$0.099 \pm 0.013 \pm 0.003$	$0.111 \pm 0.008 \pm 0.004$
215.73	$0.120 \pm 0.005^{+0.016}_{-0.015}$	4.15 ± 0.12	$0.101 \pm 0.012 \pm 0.004$	$0.113 \pm 0.007 \pm 0.005$
231.88	$0.122 \pm 0.006^{+0.015}_{-0.014}$	4.22 ± 0.11	$0.102 \pm 0.011 \pm 0.004$	$0.116 \pm 0.007 \pm 0.005$
246.86	$0.121 \pm 0.008^{+0.016}_{-0.015}$	4.32 ± 0.11	$0.101 \pm 0.012 \pm 0.004$	$0.116 \pm 0.008 \pm 0.005$
264.86	$0.115 \pm 0.011^{+0.016}_{-0.015}$	4.17 ± 0.10	$0.097 \pm 0.014 \pm 0.003$	$0.112 \pm 0.010 \pm 0.004$
281.96	$0.140 \pm 0.013^{+0.014}_{-0.013}$	4.31 ± 0.10	$0.114 \pm 0.013 \pm 0.005$	$0.137 \pm 0.011 \pm 0.008$
302.22	$0.137 \pm 0.022^{+0.014}_{-0.013}$	4.28 ± 0.09	$0.112 \pm 0.019 \pm 0.005$	$0.136 \pm 0.019 \pm 0.007$
322.87	$0.124 \pm 0.035^{+0.016}_{-0.015}$	4.60 ± 0.09	$0.103 \pm 0.028 \pm 0.004$	$0.123 \pm 0.032 \pm 0.006$
343.88	$0.154 \pm 0.056^{+0.016}_{-0.014}$	4.55 ± 0.08	$0.123 \pm 0.041 \pm 0.006$	$0.155 \pm 0.056 \pm 0.010$
380.72	$0.161 \pm 0.101^{+0.016}_{-0.014}$	4.66 ± 0.07	$0.127 \pm 0.078 \pm 0.007$	$0.166 \pm 0.109 \pm 0.012$
418.55	$0.188 \pm 0.143^{+0.018}_{-0.017}$	4.86 ± 0.07	$0.144 \pm 0.224 \pm 0.010$	$0.201 \pm 0.251 \pm 0.020$

Table 1: The extracted leading order $\alpha_S^{(0)}$ with statistical and systematical errors based on the published CDF data [23]. The higher order coefficient k_1 for $\mu_R = \mu_F = E_T$ is also shown with its associated MC-integration error. The last two columns give $\alpha_S^{(1)}$ based on the solution of eq. 12 with the combined statistical/systematic errors from [23] and the theoretical uncertainty estimate using method I as described in the text.

In fig. 2 we show both the exact $\Delta\alpha_S(\lambda)/\alpha_S$ defined by eq. 14 and its logarithmic tangent as given by eq. 16 for one E_T -bin. We see that for $0.5 < \lambda < 2$, the linear approximation is reasonable. The extracted values of $\alpha_S^{(1)}(E_T)$ (with the associated theoretical errors) defined by eqs. 17 and 18 for the 38 transverse energy bins are given in Table 1. Numerically, the major difference between the two methods of estimating the theoretical uncertainty is that in method I the estimated theoretical uncertainty is of the order of 4%, while method II gives a smaller theoretical uncertainty of typically 2%. The central value of $\alpha_S^{(1)}(E_T)$ using method II is lower by 2%, but remains within the uncertainty of method I. For the rest of the paper we will use the $\alpha_S(E_T)$ extraction based on method I. As a rough guide, changing to method II means reducing the theoretical uncertainty and lowering the central value by 2%.

5.2 Measurement of $\alpha_S^{(1)}(M_Z)$

The next step is to determine the strong coupling constant at M_Z by evolving from $\mu_R = E_T$ to $\mu_R = M_Z$ using the 2-loop evolution equation eq. 3. To extract the common long range systematic error, $\Delta\alpha_S^{sys}$, we employed the following ad hoc procedure. Because $\alpha_S(M_Z; \mu_R = E_T)$ is supposed to be independent of E_T we can define $\Delta\alpha_S^{sys}$ such that,

$$\chi^2 = \frac{1}{N_{bins}} \sum_{i=1}^{N_{bins}} \frac{[\alpha_S^{(1)}(M_Z; \mu_R = E_T^{(i)}) - \langle \alpha_S(M_Z) \rangle]^2}{[\Delta\alpha_S^{exp}(M_Z; \mu_R = E_T^{(i)}) - \Delta\alpha_S^{sys}]^2} = 1. \quad (20)$$

Here $E_T^{(i)}$ refers to the specific bin-values. This procedure gives us a value for $\Delta\alpha_S^{sys} = 0.008$, which is then common to all values of α_S . The remaining errors, $\Delta\alpha_S^{stat} = \Delta\alpha_S^{exp} - \Delta\alpha_S^{sys}$, are a combination of statistical errors and shorter range correlated systematic errors. Fig. 3 and Table 1 display the values of $\alpha_S(M_Z)$ extracted from the 38 E_T bins with the associated experimental statistical error and the estimate of the theoretical uncertainty. The systematic error is an overall factor of ± 0.008 . We see that measured value of $\alpha_S(M_Z)$ is essentially independent of E_T for the MRSA' parton density functions. This is also true of the MRSD0' and MRSD-' parameterisations.

5.3 The QCD-fit to $\alpha_S^{(1)}(M_Z)$

To compare the obtained result with QCD we first assume that next-to-leading order QCD is sufficient to describe the data. In this case $\partial\alpha_S(M_Z; \mu_R = E_T)/\partial E_T = 0$ and we can perform an error weighted average to obtain the average $\alpha_S^{(1)}(M_Z)$,

$$\alpha_S^{(1)}(M_Z) = \frac{1}{w} \sum_{i=1}^{N_{bins}} w_i \alpha_S^{(1)}(M_Z; \mu_R = E_T^{(i)}), \quad (21)$$

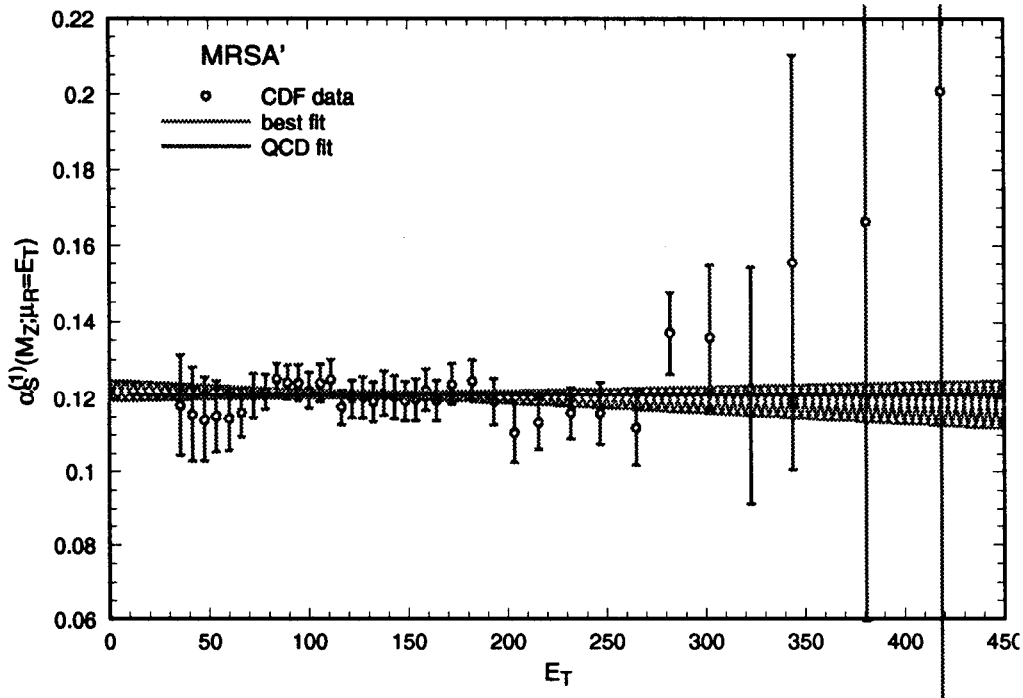


Figure 3: The extracted $\alpha_S^{(1)}(M_Z, \mu_R = E_T)$ as a function of E_T for the MRSA' parameterisation. The QCD-fit yields $\alpha_S^{(1)}(M_Z) = 0.121 \pm 0.001 \pm 0.008 \pm 0.005$. The 68% confidence level Best-fits are shown as shaded bands.

where,

$$\frac{1}{w_i} = \Delta\alpha_S^{stat}(M_Z; \mu_R = E_T^{(i)}),$$

$$w = \sum_{i=1}^{N_{bins}} w_i. \quad (22)$$

The resulting values for $\alpha_S^{(1)}(M_Z)$ are,

$$\begin{aligned} \alpha_S^{(1)}(M_Z) &= 0.119 \pm 0.001 \pm 0.008 \pm 0.005 \text{ for MRSD0'} \\ \alpha_S^{(1)}(M_Z) &= 0.121 \pm 0.001 \pm 0.008 \pm 0.005 \text{ for MRSA'} \\ \alpha_S^{(1)}(M_Z) &= 0.124 \pm 0.001 \pm 0.008 \pm 0.005 \text{ for MRSD-'} \end{aligned} \quad (23)$$

where the first error is the statistical error, the second error the systematic error and the third error the theoretical uncertainty estimate based on method I⁵. We see that the error from using different PDF as input is approximately ± 0.002 .

A note of caution is in order. In the analysis presented here, we have taken PDF's which have a Q^2 evolution based on $\alpha_S^{DIS}(M_Z) = 0.113 \pm 0.005$ [6], while the explicit α_S in the

⁵Using method II would lower $\alpha_S(M_Z)$ by 0.003 and reduce the theoretical uncertainty to 0.003

PDF	a	b	c	d
MRSD0'	0.119	0.0038	0.0008	11.0
MRSA'	0.120	-0.0010	0.0010	6.8
MRSD-'	0.124	-0.0014	0.0011	6.2

Table 2: Best-fit results from minimum χ^2 -fit

matrix elements was varied. This can only be consistent if the extracted value of $\alpha_S(M_Z)$ is in agreement with $\alpha_S^{DIS}(M_Z)$. However, we see that this is indeed the case (c.f. 23) once the statistical, systematic and theoretical errors are combined. With the new high statistic data sets of run 1A/B, the statistical and systematic errors will be significantly reduced and it will be necessary to utilise PDF's with Q^2 evolution for a variety of $\alpha_S(M_Z)$ values. Recently such PDF sets have come available [32, 33] so that a more consistent determination of α_S will be possible once the new data becomes available.

5.4 The Best-fit to $\alpha_S^{(1)}(M_Z)$

The second comparison with QCD we can perform is a check on the running behavior of α_S . For such a check, the overall systematic error is not important and the experimental error is reduced considerably. This tests whether $\alpha_S(M_Z)$ is independent of the distance scale at which the scattering takes place. To do this we no longer assume $\partial\alpha_S(M_Z; \mu_R = E_T)/\partial E_T = 0$ but allow it to be a constant. If QCD is correct, the constant should be zero within errors. The results from a minimal χ^2 fit to a linear function in E_T ,

$$\begin{aligned} \alpha_S^{(1)}(M_Z; \mu_R = E_T) &= a + b \times \left(\frac{E_T}{E_T^0} - 1 \right) \\ \Delta\alpha_S^{stat}(M_Z; \mu_R = E_T) &= c \times \sqrt{1 + d \times \left(\frac{E_T}{E_T^0} - 1 \right)^2}, \end{aligned} \quad (24)$$

are given in Table 2 for the MRSD0', MRSA' and MRSD-' parameterisations. The scale $E_T^0 \simeq 130$ GeV gives the minimal one-sigma error. The common systematic error, $\Delta\alpha_S^{sys} = 0.008$ is not affected by the fits. The linear minimal- χ^2 fits give a perfect fit to QCD (i.e. no E_T dependence) within one sigma over a range from 30 GeV to 500 GeV for MRSA' and MRSD-', while the MRSD0' results show a small but insignificant dependence on the transverse energy which possibly indicate some problems with the underlying PDF set. It should be stressed that these results are highly non trivial and demonstrate the correctness of QCD over a wide range of momentum transfers (or distance scales) not previously probed. Although the statistics are rather poor at high E_T , the new CDF and DØ results should give better results in the region above 200 GeV.

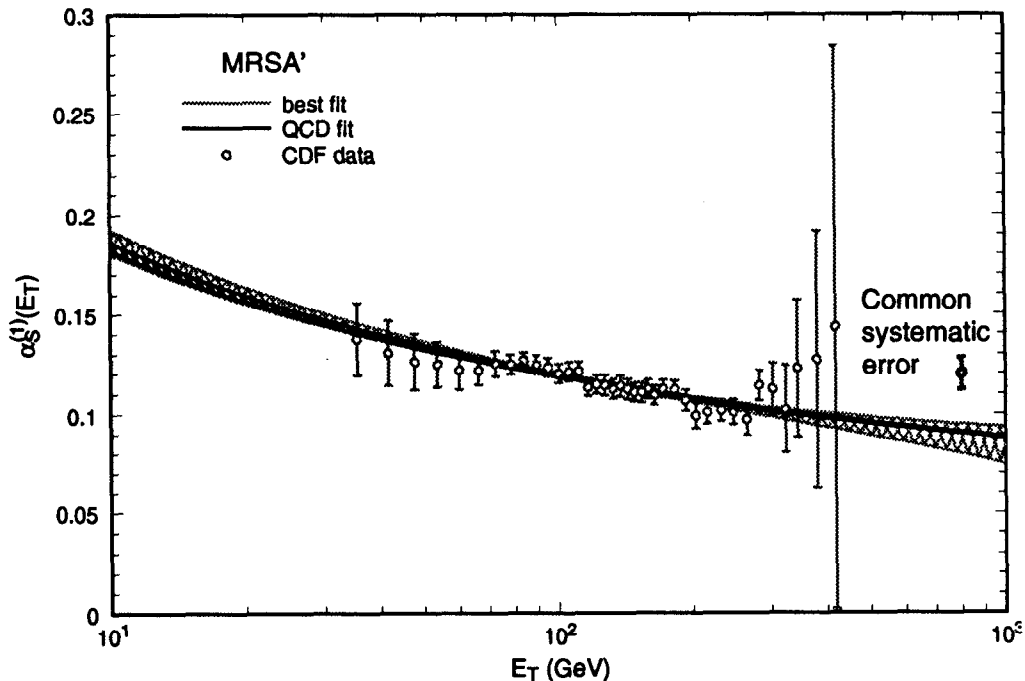


Figure 4: The values of $\alpha_S^{(1)}(E_T)$ extracted from the published CDF data as a function of E_T together with $\alpha_S^{(1)}(E_T)$ from the QCD- and Best-fits evolved from M_Z to E_T for the MRSA' parameterisation.

Next we can evolve the Best-fit result from $\alpha_S(M_Z; \mu_R = E_T)$ back to $\alpha_S(E_T)$ and extrapolate to smaller and larger E_T values to obtain the measured running α_S and then compare that with the QCD prediction from the QCD-fit. This comparison is shown in fig. 4 where we can see that the measured evolution agrees perfectly with the QCD evolution for the MRSA' parameterisation. On the other hand, if we use the Best-fit for the MRSD0' set, we find a slower running of the coupling constant which agrees very well with, in particular, the low energy α_S measurements [25]. The results from the new collider run will clarify this and test the running α_S behavior much better.

Finally, we can use the measured evolution of α_S to calculate the one-jet inclusive cross section. The differential distribution is shown in fig. 5, while the more useful data divided by theory result is shown in fig. 6. Both the QCD-fit (including the systematic error) and the Best-fit for the MRSA' parameterisation describe the data well. The prescaling thresholds and systematic errors are clearly visible.

Note that if we use the measured running α_S for other predictions and compare to the CDF '88-'89 data set results the common luminosity error would cancel because it is parametrized in the measured α_S .

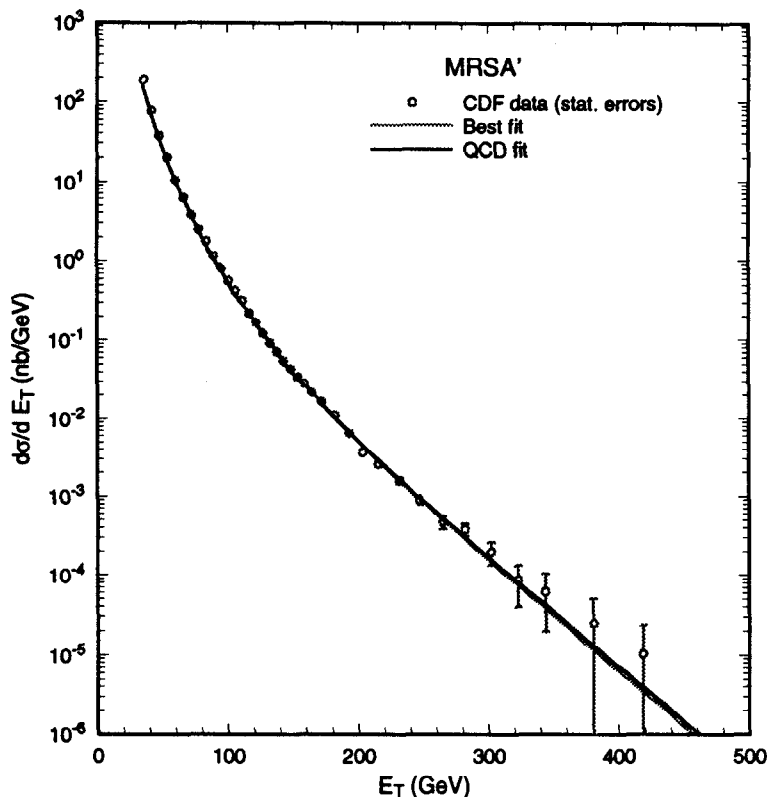


Figure 5: Comparison of the one-jet inclusive transverse energy distribution evaluated using $\alpha_S^{(1)}(E_T)$ from the QCD- and Best-fits evolved from M_Z to E_T for the MRSA' parameterisation.

6 Conclusions

In this paper we have made a first study of the ability of a hadron collider experiment to extract α_S and have utilised the unique feature of hadron colliders to measure α_S over a wide range of momentum transfers. As an example we examined the one-jet inclusive transverse energy distribution and used the CDF '88-'89 data with an integrated luminosity of 4.2 pb^{-1} . There are two main conclusions. First, the extracted $\alpha_S(M_Z)$ was consistent with the DIS value of α_S used as an input in the Q^2 evolution of the parton density functions. In the future, one can extend this method to include simultaneous variation of α_S in both the PDF's and the hard scattering cross section. Second, the measured evolution of α_S , as function of the momentum transfer in the scattering, was shown to be consistent with QCD predictions from 30 GeV up to 500 GeV.

The published data suffers from large systematic errors. However, the current run at Fermilab should deliver in excess of 100 pb^{-1} to both the CDF and DØ experiments. This should significantly reduce the error on the extracted α_S and on its running behavior. Fur-

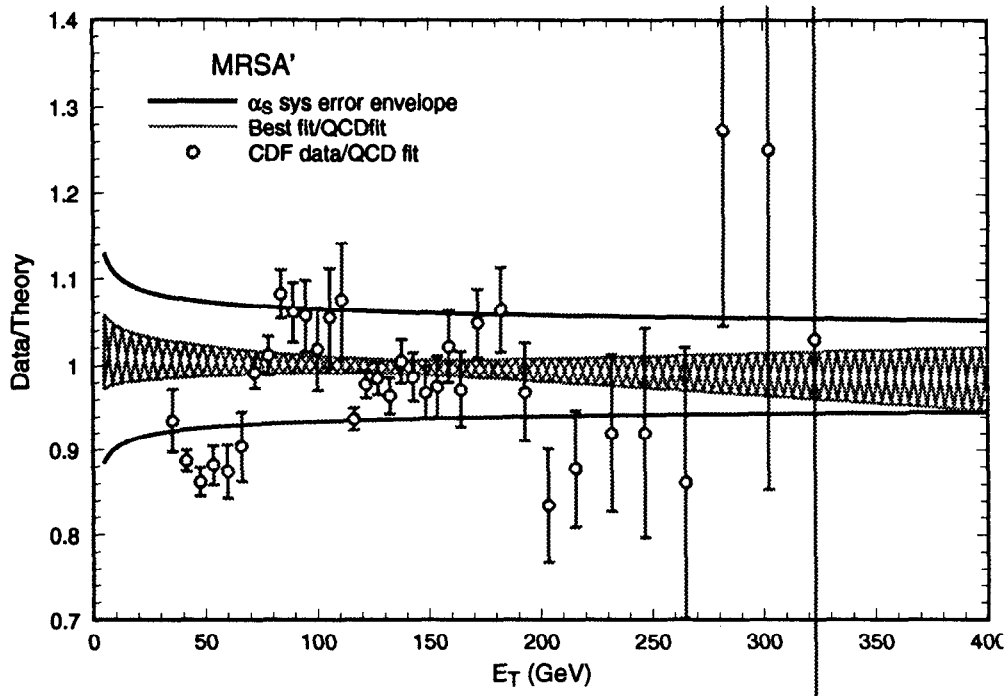


Figure 6: Ratio of the published CDF data and next-to-leading order prediction evaluated using $\alpha_S^{(1)}(E_T)$ from the QCD- and Best-fits evolved from M_Z to E_T for the MRSA' parameterisation. The systematic uncertainty is also shown in the QCD-fit based procedure.

thermore, the high luminosity offers other possibilities to measure α_S with high precision, for example in high momentum Z -boson production which requires only the measurement of the charged lepton momenta. With the forthcoming main injector program at Fermilab and an integrated luminosity well over 1000 pb^{-1} , the α_S measurements will keep improving significantly in the coming years.

Finally, with such a high luminosity it will be possible to measure the PDF's at high Q^2 and moderate x values with no input from other experiments. This, combined with the α_S -measurement, will form a precise test of QCD. As one makes a high statistic probe of distance scales, hitherto only partially explored, any deviations from QCD at high momentum transfers should become apparent and possible shortcomings in the theory should be identified. In the long term, the LHC will be an excellent machine to both measure α_S up to very high momentum transfers (up to around 5 TeV) as well as the PDF's at higher Q^2 and lower x .

Acknowledgements

We thank the CDF and DØ collaboration for their help in completing this analysis. WTG thanks Dr. B. Bardeen and Prof. S. Bethke for many useful discussions. EWNG thanks the Fermilab theory group for its kind hospitality where this work was initiated. JY expresses his appreciation to Prof. H. Weerts for many useful discussions and to the National Science Foundation of the US government for support in this investigation

References

- [1] C. S. Mishra, Proceedings of Division of Particles and Fields '92, World Scientific, eds. C. H. Albright, P. H. Casper, R. Raja, and J. Yoh, 1619 (1993).
- [2] DELPHI Collab., P. Abreu et al., Phys. Lett. **B255**, 466 (1991); Z. Phys. **C59**, 357 (1993);
ALEPH Collab., D. Decamp et al., Phys. Lett. **B284**, 151 (1992);
OPAL Collab., R. Akers et al., Z. Phys. **C65**, 367 (1995).
- [3] A. D. Martin, R. G. Roberts and W. J. Stirling, Phys. Lett. **B306**, 145 (1993).
- [4] CTEQ Collab., H. L. Lai et al., Phys. Rev. **D51**, 4763 (1995).
- [5] M. Gluck, E. Reya and A. Vogt, University of Dortmund preprint, DO-TH-94-24.
- [6] A. D. Martin, R. G. Roberts and W. J. Stirling, Phys. Rev. **D50**, 6734 (1994); Durham University preprint DTP/95/14.
- [7] UA1 Collab., G. Arnison et al., Phys. Lett. **B136**, 294 (1984).
- [8] CDF Collaboration, F. Abe et al., Fermilab preprints, FERMILAB-CONF-93/203-E, FERMILAB-CONF-94/144-E;
CDF Collaboration, presented by Eve Kovacs, Eighth Meeting of the Division of Particles and Fields of the American Physical Society, Albuquerque, New Mexico, August 1994, Fermilab preprint FERMILAB-CONF-94/215-E;
CDF collaboration, presented by Freedy Nang, Tenth Topical Workshop on Proton – Anti-proton Collider Physics, Fermilab, May 1995.
- [9] W. T. Giele, E. W. N. Glover and D. A. Kosower, Phys. Lett. **B339**, 181 (1994).
- [10] A. D. Martin, R. G. Roberts and W. J. Stirling, Phys. Lett. **B318**, 184 (1993).
- [11] D0 Collaboration, presented by Harry Weerts, Ninth Topical Workshop on Proton – Anti-proton Collider Physics, Tsukuba, Fermilab preprint, FERMILAB-CONF-94/35-E.

- [12] D0 collaboration, presented by Freedy Nang, Eighth Meeting of the Division of Particles and Fields of the American Physical Society, Albuquerque, New Mexico, August 1994, Fermilab preprint FERMILAB-CONF-94-341-E;
D0 collaboration, presented by T. L. Geld, XXXth Rencontres de Moriond, Les Arcs, March 1995;
D0 collaboration, presented by Freedy Nang, Tenth Topical Workshop on Proton – Anti-proton Collider Physics, Fermilab, May 1995.
- [13] W. T. Giele, E. W. N. Glover and D. A. Kosower, Fermilab preprint FERMILAB-PUB-94-382-T, to appear in Phys. Rev. D.
- [14] S. D. Ellis and D. E. Soper, University of Oregon preprint OITS-565.
- [15] W. T. Giele and E. W. N. Glover, talks presented at XXXth Rencontres de Moriond, Les Arcs, March 1995 and Tenth Topical Workshop on Proton – Anti-proton Collider Physics, Fermilab, May 1995, Fermilab preprints FERMILAB-CONF-95-168-T and FERMILAB-CONF-95-169-T.
- [16] UA2 Collab., J. Alitti et al., Phys. Lett. **B215**, 175 (1988), Phys. Lett. **B263**, 563 (1991).
- [17] UA1 Collab., M. Lindgren et al, Phys. Rev. **D45**, 3038 (1992).
- [18] DØ Collab., S. Abachi et al., Fermilab preprint FERMILAB-PUB-95-085-E;
D0 collaboration, presented by J. Yu, Tenth Topical Workshop on Proton – Anti-proton Collider Physics, Fermilab, May 1995.
- [19] D. J. Gross and F. Wilczek, Phys. Rev. Lett. **30**, 1343 (1973); Phys. Rev. **D8**, 3633 (1973);
H. D. Politzer, Phys. Rev. Lett. **30**, 1346 (1973).
- [20] W. Caswell, Phys. Rev. Lett. **33**, 244 (1974);
D. R. T. Jones, Nucl. Phys. **B75**, 531 (1974).
- [21] O. V. Tarasov, A. A. Vladimorov and A. Yu. Zharkov, Phys. Lett. **B93**, 429 (1980).
- [22] S. D. Ellis, Z. Kunszt and D. E. Soper, Phys. Rev. **D40**, 2188 (1989); Phys. Rev. Lett. **64**, 2121 (1990).
- [23] CDF Collab., F. Abe et al., Phys. Rev. Lett. **68**, 1104 (1992).
- [24] R. Hamberg, W. L. van Neerven and T. Matsuura, Nucl. Phys. **B359**, 343 (1991).
- [25] See for example, B. R. Webber, Plenary talk at XXVII International Conference on High Energy Physics, Glasgow, July 1994. or S. Bethke, University of Aachen preprint PITHA 94/30, talk presented at QCD '94, Montpellier, France, July 1994.
- [26] CDF Collab., Fermilab preprint FERMILAB-PUB-91-231-E.

- [27] See, for example, J. E. Huth et al., in Research Directions for the Decade, Proceedings of the 1990 Division of Particles and Fields Summer Study, Snowmass, 1990, edited by E. L. Berger (World Scientific, Singapore, 1992), p.134.
- [28] W. T. Giele, E. W. N. Glover and D. A. Kosower, Phys. Rev. Lett. **73**, 2019 (1994).
- [29] W. T. Giele and E. W. N. Glover, Phys. Rev. **D46**, 1980 (1992).
- [30] W. T. Giele, E. W. N. Glover and D. A. Kosower, Nucl. Phys. **B403**, 633 (1993).
- [31] R. K. Ellis and J. Sexton, Nucl. Phys. **B269**, 445 (1986).
- [32] A. Vogt, Desy preprint DESY-95-068.
- [33] A. D. Martin, R. G. Roberts and W. J. Stirling, Durham University preprint DTP/95/48.